REPORT DOCUMENTATION PAGE

Form Approved OMB NO. 0704-0188

1. REPORT DATE (DD-MM-YYYY)	2. REPORT TYPE	3. DATES COVERED (From - To)
02-08-2014	Final Report	18-May-2009 - 17-Feb-2014

4. TITLE AND SUBTITLE
Molecular transporters for desalination applications

5a. CONTRACT NUMBER
W911NF-09-1-0267

5b. GRANT NUMBER

5c. PROGRAM ELEMENT NUMBER
8G10AV

6. AUTHORS
Bruce Hinds

5d. PROJECT NUMBER

5e. TASK NUMBER

5f. WORK UNIT NUMBER

7. PERFORMING ORGANIZATION NAMES AND ADDRESSES
University of Kentucky
500 South Limestone Street
109 Kinkead Hall
Lexington, KY 40526 -0001

8. PERFORMING ORGANIZATION REPORT NUMBER

9. SPONSORING/MONITORING AGENCY NAME(S) AND ADDRESS (ES)
U.S. Army Research Office
P.O. Box 12211
Research Triangle Park, NC 27709-2211

10. SPONSOR/MONITOR'S ACRONYM(S)
ARO

11. SPONSOR/MONITOR'S REPORT NUMBER(S)
56386-EV-DRP.14

12. DISTRIBUTION AVAILIBILITY STATEMENT
Approved for Public Release; Distribution Unlimited

13. SUPPLEMENTARY NOTES
The views, opinions and/or findings contained in this report are those of the author(s) and should not contrued as an official Department of the Army position, policy or decision, unless so designated by other documentation.

14. ABSTRACT
The primary goal of the 'Molecular Transporter' program was to develop a precise platform to mimic protein channels and enzyme reaction sites. In particular a grand challenge is to orientate the target substrate molecule with angstrom scale precision of functional placement at pore entrances. Notable examples in nature are the aquaporin channel that can flip the orientation of pure water target 180o and thus prevent hydronium ion (i.e. pH) passage as well as ion exclusion. Nearly all enzyme catalyst require precise substrate binding sites that allow precise placement of reaction bond over catalyst site. Furthermore protein channels support dramatic nanofluidic flow

15. SUBJECT TERMS
desalination biomimetric membranes activated chemical transport

16. SECURITY CLASSIFICATION OF:			17. LIMITATION OF ABSTRACT	15. NUMBER OF PAGES	19a. NAME OF RESPONSIBLE PERSON
a. REPORT	b. ABSTRACT	c. THIS PAGE			Bruce Hinds
UU	UU	UU	UU		19b. TELEPHONE NUMBER 859-218-6543

Report Title

Molecular transporters for desalination applications

ABSTRACT

The primary goal of the 'Molecular Transporter' program was to develop a precise platform to mimic protein channels and enzyme reaction sites. In particular a grand challenge is to orientate the target substrate molecule with angstrom scale precision of functional placement at pore entrances. Notable examples in nature are the aquaporin channel that can flip the orientation of pure water target 180o and thus prevent hydronium ion (i.e. pH) passage as well as ion exclusion. Nearly all enzyme catalyst require precise substrate binding sites that allow precise placement of reaction bond over catalyst site. Furthermore protein channels support dramatic nanofluidic flow enhancement due to the ordering of fluid through channel and short path length across the lipid bi-layer. The approach here was to have single wall carbon nanotubes (SWCNT) with exact (stoichiometric) diameter control serve as platform for bio-mimetic gatekeepers. In particular mimicking aquaporin channels with a single-file column of water passing through CNT core that supports near perfect slip boundary flow. Of particular importance to DoD mission is to have compact and energy efficient desalination units. In particular with CNTs of ~2wt% loading, 100 fold reduction in membrane area is expected.

Enter List of papers submitted or published that acknowledge ARO support from the start of the project to the date of this printing. List the papers, including journal references, in the following categories:

(a) Papers published in peer-reviewed journals (N/A for none)

Received		Paper
05/15/2013	8.00	Ji Wu, Karen Gerstandt, Mainak Majumder, Xin Zhan, Bruce J. Hinds. Highly efficient electroosmotic flow through functionalized carbon nanotube membranes, Nanoscale, (2011): 0. doi: 10.1039/c1nr10303b
08/31/2012	1.00	Kathryn E. deKrafft, Cheng Wang, Zhigang Xie, Xin Su, Bruce J. Hinds, Wenbin Lin. Electrochemical Water Oxidation with Carbon-Grafted Iridium Complexes, ACS Applied Materials & Interfaces, (02 2012): 0. doi: 10.1021/am2018095
08/31/2012	5.00	Jacob Goldsmith, Bruce J. Hinds. Simulation of Steady-State Methanol Flux through a Model Carbon Nanotube Catalyst Support, The Journal of Physical Chemistry C, (10 2011): 0. doi: 10.1021/jp201467y
08/31/2012	4.00	Xin Su, Xin Zhan, Bruce J. Hinds. Pt monolayer deposition onto carbon nanotube mattes with high electrochemical activity, Journal of Materials Chemistry, (2012): 0. doi: 10.1039/c2jm15395e
08/31/2012	3.00	Bruce Hinds. Dramatic transport properties of carbon nanotube membranes for a robust protein channel mimetic platform, Current Opinion in Solid State and Materials Science, (02 2012): 0. doi: 10.1016/j.cossms.2011.05.003
08/31/2012	2.00	Bruce J. Hinds, Jie Liu, Karen Gerstandt, Hongbo Zhang, Ji Wu. Electrophoretically induced aqueous flow through single-walled carbon nanotube membranes, Nature Nanotechnology, (01 2012): 0. doi: 10.1038/nnano.2011.240
10/14/2013	11.00	Xin Zhan, Ji Wu, Zhiqiang Chen, Bruce J Hinds. Single-step electrochemical functionalization of double-walled carbon nanotube (DWCNT) membranes and the demonstration of ionic rectification, Nanoscale Research Letters, (06 2013): 279. doi: 10.1186/1556-276X-8-279
10/14/2013	12.00	Xinghua Sun, Ji Wu, Zhiqiang Chen, Xin Su, Bruce J. Hinds. Fouling Characteristics and Electrochemical Recovery of Carbon Nanotube Membranes, Advanced Functional Materials, (03 2013): 1500. doi: 10.1002/adfm.201201265
10/14/2013	13.00	Ji Wu, Xin Zhan, Bruce J. Hinds. Ionic rectification by electrostatically actuated tethers on single walled carbon nanotube membranes, Chemical Communications, (06 2012): 7979. doi: 10.1039/c2cc33355d
TOTAL:		**9**

Number of Papers published in peer-reviewed journals:

(b) Papers published in non-peer-reviewed journals (N/A for none)

Received	Paper

TOTAL:

Number of Papers published in non peer-reviewed journals:

(c) Presentations

Presentations:
Invited:
'Dramatic Nano-Fluidic Properties of Carbon Nanotube Membranes as a Platform for Protein Channel Mimetic Pumps' Gordon Res. Conf., Graphitic Carbon Materials, Bates Coll., June 2014
'Dramatic nano-fluidic properties of carbon nanotube membranes as a platform for protein channel mimetics' Dept. of Mech Engr, Univ. Washington, May 2014
'Dramatic nano-fluidic properties of carbon nanotube membranes for biomimetic desalination application' Blue Tech Webinar Series, May 2014
'Dramatic nano-fluidic properties of carbon nanotube membranes as a platform for protein channel mimetics' Dept. of Mater. Sci. Engr, Univ. Washington, April 2014
'Dramatic nano-fluidic properties of carbon nanotube membranes as a platform for protein channel mimetics' Dept. of Chemistry, Colorado School of Mines, April 2014
'Gated carbon nanotube membranes for counseling enhanced transdermal addiction therapy' American Association for Nanomedicine, Bethesda MD March 2014
'Remotely programmed transdermal delivery through voltage gated carbon nanotube membranes for counseling enhanced addiction treatment' Addiction Therapy and Treatment, Las Vegas NV July, 2013
'Dramatic nano-fluid and electro-active properties of carbon nanotube membranes' American Physics Society March Meeting, Baltimore MD, March 2013
'Dramatic nano-fluid and electro-active properties of carbon nanotube membranes' Dept. Mater. Sci. Engr. University of Washington, Seattle WA, Feb 2013
'Dramatic nano-fluid and electro-active properties of carbon nanotube membranes' 1st Bielefeld workshop on nanolayers and artificial membranes, Bielefeld German, Feb. 2013
'Dramatic nano-fluid and electro-active properties of carbon nanotube membranes' French American Innovation Day: Membrane Technologies as Tools for Sustainability in Water Management, MIT Boston MA, Nov. 2012
'Dramatic nano-fluidic properties of carbon nanotube membranes as a platform for protein channel mimetics' Univ. Missouri St Louis, Oct. 2012
'Dramatic nano-fluidic properties of carbon nanotube membranes as a platform for protein channel mimetics' Univ. Ill. Chicago Sept. 2012
'Water Treatment Opportunities Utilizing the Dramatic Nano-Fluidic Properties of Carbon Nanotube Membranes' AIChE, Minneapolis MN, Nov 2011
'Dramatic nano-fluidic properties of carbon nanotube membranes', Univ. Montpellier., July 8 2011
'Dramatic nano-fluidic properties of carbon nanotube membranes and their use in programmable drug delivery', Dept. Mater. Sci. Eng., Northwestern Univ., May 10 2011
'Dramatic nano-fluidic properties of carbon nanotube membranes and their use in programmable drug delivery', PacifiChem, Honolulu, Dec. 16 2010
'Programmed transdermal delivery of addictive substances through voltage gated carbon nanotube membranes' American College of Neuropsychopharmacology, Orlando Dec. 5 2010
'Dramatic nano-fluidic properties of carbon nanotube membranes and their use in programmable drug delivery' Univ. of Akron, Nov 18 2010
'Kavli Frontiers of Science Symposia Faculty Participant' National Academy of Sciences, Irvine CA, Nov. 4 – 6 2010
'Dramatic nano-fluidic properties of carbon nanotube membranes' Korean CNT-membrane Forum' full travel support, Seoul National University, Oct. 14-15th 2010
'Dramatic nano-fluidic properties of carbon nanotube membranes and their use in programmable drug delivery' Dept. of Mech. Engr., Ohio State Univ. Oct. 3, 2010
'Dramatic nano-fluidic properties of carbon nanotube membranes and their use in programmable drug delivery', Dept. of Chem. Engr., Virginia Polytechnic Institute, Sept 22, 2010
'Workshop: Emerging Membrane Materials and Manufacturing methods' North American Membrane Society, July 18, 2010 (highest paid attendance of offered workshops)
'Highly efficient electro-osmotic flow through carbon nanotube membranes' Fundamentals of Nanotechnology, Salt Lake City, April 29, 2010
'Programmed transdermal drug delivery with carbon nanotube membranes: using dramatic nano-scale properties for addiction treatment' Department of Chemistry, Duke University April 12, 2010
'Active carbon nanotube membranes for programmed transdermal addiction treatment' Society for Research on Nicotine and Tobacco (NIH-NIDA sponsored) Feb. 24, 2010
'Aligned Carbon nanotubes: flow enhancement and gatekeeper activity' European Membrane Society Meeting, Mount Pellier Fr. Sept. 1-10, 2009 (keynote talk, emerging membrane materials workshop, young investigator workshop)
'Workshop: Emerging Membrane Materials and Manufacturing methods' North American Membrane Society, June 22 2009 (highest paid attendance of offered workshops)
'Carbon Nanotube Membranes for Pressure Retarded Osmotic Power Generation' Statkraft Corporation, Oslo Norway June 5 2009
'Aligned Carbon nanotubes: flow enhancement and gatekeeper activity' IGERT Seminar, Univ. Massachusetts Amherst, May 7 2009
'Aligned Carbon nanotubes: flow enhancement and gatekeeper activity' Lawrence Berkeley Laboratory March 5 2009

Number of Presentations: 30.00

Non Peer-Reviewed Conference Proceeding publications (other than abstracts):

Received Paper

TOTAL:

Number of Non Peer-Reviewed Conference Proceeding publications (other than abstracts):

Peer-Reviewed Conference Proceeding publications (other than abstracts):

Received Paper

TOTAL:

Number of Peer-Reviewed Conference Proceeding publications (other than abstracts):

(d) Manuscripts

Received Paper

TOTAL:

Number of Manuscripts:

Books

Received Book

TOTAL:

Received	Book Chapter

TOTAL:

Patents Submitted

Patents Awarded

Awards

Visiting Professor, University of Montpellier 2011
Kavli Frontiers of Science Fellow, National Academy of Science 2010
Elected vice-chair Gordon Conference 'Membranes: Materials & Processes 2012', Chair 2014
Presidential Early Career Award (PECASE, NIH) 2009

Graduate Students

NAME	PERCENT_SUPPORTED	Discipline
Xin Su	0.75	
Xhin Zhan	0.75	
Nick Linck	0.50	
Karen Gerstandt	0.50	
Jingyuan Yao	0.90	
Zhiqiang Chen	0.10	
FTE Equivalent:	**3.50**	
Total Number:	**6**	

Names of Post Doctorates

NAME	PERCENT_SUPPORTED
Ji Wu	0.20
Xin Su	0.80
FTE Equivalent:	**1.00**
Total Number:	**2**

Names of Faculty Supported

NAME	PERCENT_SUPPORTED	National Academy Member
Bruce Hinds	0.15	
FTE Equivalent:	**0.15**	
Total Number:	**1**	

Names of Under Graduate students supported

NAME	PERCENT_SUPPORTED
FTE Equivalent:	
Total Number:	

Student Metrics

This section only applies to graduating undergraduates supported by this agreement in this reporting period

The number of undergraduates funded by this agreement who graduated during this period:	0.00
The number of undergraduates funded by this agreement who graduated during this period with a degree in science, mathematics, engineering, or technology fields:.....	0.00
The number of undergraduates funded by your agreement who graduated during this period and will continue to pursue a graduate or Ph.D. degree in science, mathematics, engineering, or technology fields:.....	0.00
Number of graduating undergraduates who achieved a 3.5 GPA to 4.0 (4.0 max scale):.....	0.00
Number of graduating undergraduates funded by a DoD funded Center of Excellence grant for Education, Research and Engineering:.....	0.00
The number of undergraduates funded by your agreement who graduated during this period and intend to work for the Department of Defense	0.00
The number of undergraduates funded by your agreement who graduated during this period and will receive scholarships or fellowships for further studies in science, mathematics, engineering or technology fields:	0.00

Names of Personnel receiving masters degrees

NAME	
Karen Gerstandt	
Jingyuan Yao	
Nick Linck	
Total Number:	**3**

Names of personnel receiving PHDs

NAME	
Xin Su	
Xin Zhang	
Zhiqiang Chen	
Total Number:	**3**

Names of other research staff

NAME	PERCENT_SUPPORTED
FTE Equivalent:	
Total Number:	

Sub Contractors (DD882)

Inventions (DD882)

Scientific Progress

See Attachment

Technology Transfer

Molecular transporters: Final Report

Bruce Hinds

Univ. of KY, Depart. of Chem. & Mater. Engr.

Present address: MSE, Univ. of Washington, bjhinds@uw.edu

Outline

I. Goals of program
II. Summary of key results and challenges
III. Publications and their relationship to program
IV. Student and young scientist mentored
V. Detailed technical results

Abstract: The primary goal of the 'Molecular Transporter' program was to develop a precise platform to mimic protein channels and enzyme reaction sites. In particular a grand challenge is to orientate the target substrate molecule with angstrom scale precision of functional placement at pore entrances. Notable examples in nature are the aquaporin channel that can flip the orientation of pure water target 180^{o} and thus prevent hydronium ion (i.e. pH) passage as well as ion exclusion. Nearly all enzyme catalyst require precise substrate binding sites that allow precise placement of reaction bond over catalyst site. Furthermore protein channels support dramatic nanofluidic flow enhancement due to the ordering of fluid through channel and short path length across the lipid bi-layer. The approach here was to have single wall carbon nanotubes (SWCNT) with exact (stoichiometric) diameter control serve as platform for bio-mimetic gatekeepers. In particular mimicking aquaporin channels with a single-file column of water passing through CNT core that supports near perfect slip boundary flow. Of particular importance to DoD mission is to have compact and energy efficient desalination units. In particular with CNTs of ~2wt% loading, 100 fold reduction in membrane area is expected.

I. Goals of program

The primary goal of the 'Molecular Transporter' program was to develop a precise platform to mimic protein channels and enzyme reaction sites. In particular a grand challenge is to orientate the target substrate molecule with angstrom scale precision of functional placement at pore entrances. Notable examples in nature are the aquaporin channel that can flip the orientation of pure water target 180^{o} and thus prevent hydronium ion (i.e. pH) passage as well as ion exclusion. Nearly all enzyme catalyst require precise substrate binding sites that allow precise placement of reaction bond over catalyst site. Furthermore protein channels support dramatic nanofluidic flow enhancement due to the ordering of fluid through channel and short path length across the lipid bi-layer. The approach here was to have single wall carbon nanotubes (SWCNT) with exact (stoichiometric) diameter control serve as platform for bio-mimetic gatekeepers. In particular mimicking aquaporin channels with a single-file column of water passing through CNT core that supports near perfect slip boundary flow.

Of particular importance to DoD mission is to have compact and energy efficient desalination units. In particular with CNTs of ~2wt% loading, 100 fold reduction in membrane area is expected. However a key scientific need was to demonstrate that CNTs can exclude ions at sea-water salt concentrations. Two approaches studied were functional chemistry with charge exclusion at pore entrance or precise SWCNT diameter control to allow only single file water flow.

The key goals are best grouped as:

'Gatekeeper' functional design

- Increased functional density
- Macromolecule zwitterion design

Precise SWCNT synthesis

- Collaborative and commercially available state-of-the-art test
- Zeolite template based synthesis

II. Summary of key results and challenges

For the key goal of 'Gatekeeper functional design' partial success was seen. Unprecedented electroosmotic flow enhancement and ionic current rectification was seen due to high charge density at CNT tips (Nat. Nano, Chem. Mater.,). In the case of electroomosis, a similar 10,000 fold flow enhancement compared to pressure driven flow was observed, thus confirming the

near perfect slip boundary conditions. However in these studies, no complete ion repulsion was seen and was consistent with prior desalination studies; That no ion exclusion at low salt concentrations of ~20mM (sea water ~800mM) was seen. The likely mechanism is the geometric problem of repulsive charge being only at the entrance. If charged at the entrance is momentarily screened then ions can enter pore and not have further hindrance traveling down the length of the pore. This is in contrast with charged ultrafiltration membranes with semi-infinite charged channels. This group had tried state of the art synthesis of zwiterions and electrochemical grafting of functional groups to achieve highest possible charge density at pore entrances. Though clear ion exclusion phenomena were seen (electroosmosis and ionic current rectification), desalination via ionic repulsion was not achieved.

In computation simulation by Corry group, it was predicted that 0.8 nm diameter CNTs would allow single-file water flow at enhanced rates while excluding ions. CNTs with ~0.9nm diameter would have fast flow through cores but not exclude ions, while CNTs at ~0.7 nm would size excludes ions but be too small to support rapid water flow. In such a case, unprecedented control of CNT diameter is needed for desalination applications. CNTs are typically grown from a transition metal catalyst nanoparticle, with its size setting CNT diameter. The tightest distribution of SWCNTs reported (Lu group, Duke Univ.) was achieved by loading catalyst into zeolite with the pore size nominally acting to set the size of catalyst on the surface. However nano particles and CNTs grow on the surface of the zeolite, thus particles can surface migrate/coalesce giving variation in diameter. Neither Duke samples nor commercially available SWCNTs showed ion rejection based on size control (but showed enhanced 'gatekeeper' effects). Our approach was to use a monolithic zeolite (VPI-5) that would set the size of the SWCNT with sub-angstrom precision due to the crystalline zeolite template. The smallest know CNTs (0.4nm diameter) were grown by a zeolite, however an important caveat was that the zeolite growth had hydrophobic channels with the organic templating agent (and carbon source) trapped within the zeolite. In our case a hydrophilic organic source, as well as catalyst had to be impregnated within the open VPI-5 structure. The unpublished work, that makes the majority of this report, shows that desired SWCNTs were made but not isolated into quantities suitable for membrane fabrication and desalination demonstration. In particular effective catalyst loading into the zeolite pore to convert carbon source into graphitic CNTs remained the largest challenge for this approach.

Though unsuccessful for desalination efforts, this research successfully laid the foundation for ionic pumps and biomimetic gatekeepers based on well controlled CNT growth methods with efficient tip functionalization.

III Publications and their relationship to program

'Single-step electrochemical functionalization of double-walled carbon nanotube membranes' X. Zhan, J Wu, B.J. Hinds *Nanoscale Research Letters* **2013** 8 279 *The purpose of this work was to have the highest yield of charged chemistry at CNT pore entrances. In prior work an electrochemical functionalization required two steps, electrochemical grafting of carboxylate chemistry then carboamide reaction of functional gatekeeper that had primary amine. In this work it was shown that primary amine could directly be electrochemically oxidized to form a covalent bond to CNT tips with density improved to the two step reaction*

'Fouling Characteristics and Electrochemical Recovery of Carbon Nanotube Membranes' X. Sun, Ji Wu, Z. Chen, X. Su and B.J. Hinds *Adv. Funct. Mater.* **2012** 23(12) 1500-06 *This work broke new ground to show that nanobubbles could be electrochemically generated at pore entrances to 'defoul' CNT membranes with the bubbles dislodging absorabates. Also applied electric field applied to membranes allowed large ions to act as brushes to clear the interior cores of CNTs. CNTs are shown to be inert to a number of typical foulants due to the 'slippery/non-interacting' nature of graphitic CNT cores.*

'Ionic Rectification by Electrostatically Actuated Tethers on Single Walled Carbon Nanotube Membranes' J. Wu, X. Zhan, B.J. Hinds *Chem Comm.* **2012** 48(64) 7979-81 *This work is the pinnacle example of charged 'gatekeepers' being able to repel small ions. Previous work had blocked large ion complexes. In this case the small/tight diameter control allowed for 1.4nm long charged and tethered molecules to be actuated with applied field to open/close the pores to small ions. Actuated molecules were larger than CNT diameter and could not be pulled inside the pore allowing for efficient gating.*

'Electrochemical Water Oxidation with Carbon-Grafted Iridium Complexes' deKrafft, K.; Wang, C.; Xie, Z.; Su, X.; Hinds, B.J.; Lin, W. *ACS Appl. Mater. & Interfaces* **2012** 4(2) 608-13. *To oxidize potential foulants, we hypothesized that Ir catalyst complexes grafted to CNT tips can split water to produce oxidants to remove foulants. As follow-on, this would solve an important problem in finding appropriate catalyst for water splitting electrochemical energy storage needs.*

'Electrophoretically Induced Aqueous Flow through sub-Nanometer Single Walled Carbon Nanotube Membranes' Ji Wu, Karen Gerstandt, Hongbo Zhang, Jie Liu, and Bruce. J. Hinds *Nature Nano* **2012** 7(2) 133-39. *This was a critical publication of the supported research, in that it confirmed the dramatic flow enhancement of atomically flat CNT cores by an independent experimental method. Under applied electric field, ions were able to accelerate solvent to generate efficient electroosmotic flow. 10,000 fold enhancement to electroosmotic velocity (m/V-s) and 100 fold improvement in power efficiency were seen, allowing for new separations driving force (as opposed to pressure and indiscriminant fouling). The study also had critical control experiments to show that transport was through CNT cores. Unfortunately this study also conclusively showed the difficulty of 'gatekeeper' ionic screening above ~20mM ion concentration requiring the need for precise CNT diameter control.*

'Dramatic Transport Properties of Carbon Nanotube Membranes for a robust protein channel mimetic platform' B.J. Hinds *Curr. Opin. in Solid. State & Mater. Sci.* **2012** 16(1) 1-9. *This review paper explained the rationale for using CNT membranes as a protein channel mimetic*

"Pt monolayer deposition onto carbon nanotube mattes with high electrochemical activity" Xin Su[#], Xin Zhan[#], Bruce J. Hinds* *J. Mater. Chem.* **2012** 22(16) 7979-84. *This work uses a newly developed Cu-underpotential method that self-limits to a monolayer of Cu(0) film that can be monotomically substituted with expensive Ptcatalyst. This approach was applied to large area outer walls of CNTs but is ultimately planned for tip-only gate keeper/catalytic CNT flow exit*.

'Highly Efficient Electro-osmotic Flow through Functionalized Carbon Nanotubes Membrane' Ji Wu, Karen Gerstandt, Mainak Majunder, B.J. Hinds, *RCS Nanoscale* **2011** 3(8) 3321-28 *This work showed the 100 fold improvement in power efficiency of using ions to pump solvent through CNTs compared to conventional materials with atomic roughness. In particular this allows a 'gate keeper' net to bind target molecules and be released from binding site and efficiently pumped through CNT by efficient electroosmotic process.*

'Simulation of steady state methanol flux through a model carbon nanotube catalyst support' Jacob Goldsmith[%] and B. J. Hinds* *J. Phys. Chem. C* **2011** 115(39) 19158-64 This work shows the preferential partition of core-flowing organics to the side wall of CNTs. As they exit they interact with Pt catalyst at tips of CNTs. This can be a higly efficient flow cell for energy or water decontamination applications.

IV Student and young scientist mentored

Xin Su, PhD MSE (Post-doc Brown Univ.)

Xin Zhan, PhD Chem (San Diego)

Zhiqiang Chen, PhD (Industry, Md)

Karen Gerstandt, MS MSE (U. Twente)

Nick Linck, MS MSE (Continuing PhD at UKy)

Jingyuan Yao, MS MSE

Ji Wu, Post doc, (Assist. Prof. S. GA Univ.)

Xin Su, Post doc (Industry, NY)

IV. Detailed technical results

Detailed technical results provided here are for unpublished work or work *in-preparation* for publication at the time of this report.

Zeolite Templated Synthesis of Carbon Nanotubes for Precise Diameter Control

Introduction

Carbon nanotube membranes composed of aligned CNTs exhibit fluid flow that is 4-5 orders of magnitude faster than conventional flow models predict. This high flow is due to the atomically flat, hydrophobic core of the carbon nanotubes[1]. Molecular dynamics simulations by Corry et al[2] show that (6,6) armchair CNTs make the optimal pores for water desalination in a CNT membrane by preventing salt ions from entering the membrane while allowing water molecules to flow single-file through the CNT core.

Previous research by Zhai et al, has demonstrated the ability to synthesize single-walled carbon nanotubes of 4Å diameter by pyrolyzing tripropylamine within the pores of AlPO4-5 zeolite[4].

- Membranes composed of aligned carbon nanotubes exhibit fluid flow that is 4-5 orders of magnitude faster than conventional flow models predict due to the atomically flat, hydrophobic core of the nanotube[1]
- Molecular dynamics simulations have shown that (6,6) armchair CNTs (d~8A) make the optimal pores for water desalination in a CNT membrane[2]
- Currently, the most common way to synthesize CNTs is by growing them on a transition metal catalyst seed particle[3-_]
- Previous research shows that the smallest known CNTs can be synthesized by pyrolysis of tripropylamine within the pores of AlPO4-5 zeolite[4]
- Virginia Polytechnic Institute number 5 (VPI-5) molecular sieve is an aluminophosphate zeolite that is similar in structure and composition to AlPO4-5, but with a larger pore size[5]

- Using the concept outlined in in the Zhai paper, it is hypothesized that we can synthesize 8A diameter CNTs by templating 1-pyrenebutyric acid as the carbon source and a cobalt nanoparticle catalyst.

Methods

VPI-5 Synthesis

Since VPI-5 zeolite is not commercially available, it was synthesized using the procedure described by Anderson, et al[6]. Alumina slurry was made by adding 30 g Catapal B alumina (Boehmite) to 47.1 g deionized water and stirred for 10 minutes. 47.25 g of 81% phosphoric acid, diluted in 30.11 g H2O was added to the slurry at approximately 3.5 cm^3/min. The mixture was then stirred using a propeller mixer for 5 minutes, followed by 2 hours of aging for the gel. After the aging process, 21.45 g of dipropylamine was added to the gel at 3.5 cm^3/min, followed by a second, two-hour aging. The hydrogel was then transferred to a Teflon-lined, stainless steel autoclave (Parr) and placed in an oven to raise the hydrogel to the crystallization temperature of 130°C. After reaching the crystallization temperature, the autoclave and hydrogel were held at this temperature without stirring for 13 hours. After the crystallization process, the autoclave was quenched in water down to room temperature. The resulting mixture was then transferred to a beaker and the VPI-5 crystals were allowed to settle. The supernatant fluid was then removed from the crystals by decantation and the resulting powder was washed five times with DI water by agitation, followed by settling and decantation. Finally, the crystals were recovered by vacuum filtration and dried at room temperature in air overnight.

Catalyst

Multiple approaches were taken to getting the activated transition metal nanoparticle catalyst into the pores of the zeolite. Variations on the procedure include the transition metal that was used as the catalyst, the location of the metal nanoparticle relative to the carbon precursor, and the oxidation state of the catalyst.

Cobalt and iron were both used as catalysts for the synthesis of carbon nanotubes. Cobalt absorption into the pores of the VPI-5 was accomplished by soaking the crystals in a solution of cobalt chloride hexahydrate ($CoCl_2 \cdot 6H_2O$) for two hours. VPI-5 zeolite with Fe3+ within the pores was synthesized via the procedure laid out by Prasad[9]. The same procedure was used to synthesize FeVPI-5 was the same as the procedure for synthesis of VPI-5 with $FeCl_3$ solution added to the hydrogel mixture after the addition of the DPA and before the second aging period.

The location of the cobalt catalyst with respect to the carbon precursor was also varied in an attempt to improve the process.

Carbon Precursor Determination

Two different compounds were considered as viable carbon sources for the synthesis of carbon nanotubes; fructose and 1-pyrenebutyric acid (PyBA). These carbon precursors were chosen based on two general criteria; that they must be hydrophilic in order to be absorbed into the hydrophilic pores of the VPI-5 and that they must contain enough carbon atoms in their structure to be able to provide a significant amount of graphitic carbon when pyrolyzed. Based on these two criteria and general

observations of the two compounds, either one could be regarded as a potential carbon source for this process.

Early synthesis attempts using fructose as the carbon source yielded poor results, and a thermodynamic study was undertaken to explain these results. This analysis was then repeated for PyBA in order to compare graphitic carbon production. It should be noted at this point that CNT growth uses a transition metal catalyst to form intermediate metal-carbides. However, these catalysts cannot perform thermodynamically unfavorable reactions and product analysis is critical. The ideally catalyzed reaction would proceed with the general form:

$$C_xH_yO_z \longrightarrow (x - \frac{y-2z}{4})C_{(s)} + \frac{y-2z}{4}CH_4 + zH_2O$$

And the two precursor compounds are shown below.

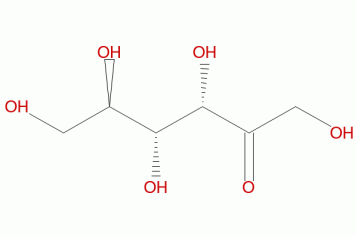

Fructose

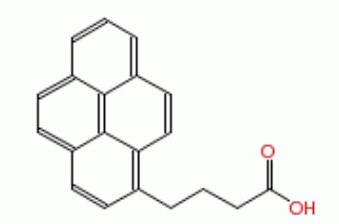

1-pyrenebutyric acid

Upon searching the literature, the most common organic products of fructose were determined and the relevant thermodynamic quantities were found using the Standard Thermodynamic Properties of Chemical Substances table from the department of chemistry at the University of Indiana[12]. The results of this search are found in Table_. Both sources listed other organics as products of the decomposition, but listing every conceivable product was not necessary to determine the proper carbon precursor.

Compound	ΔHf (kJ/mol)	S° (kJ/mol*K)	Reference
Benzene	49.0	0.1733	Higman et al[13]
Toluene	12.0	0.2210	Higman et al[13]
Phenol	-165.0	0.1440	Higman et al[13]
Ethylbenzene	-12.5	0.2550	Higman et al[13]
Styrene	103.4	0.2380	Higman et al[13]
Indene	110.6	0.2153	Higman et al[13]
Acetaldehyde	-166.2	0.2638	Fagerson et al[14]
Acetone	-217.1	0.2953	Fagerson et al[14]
Ethanol	-234.8	0.2816	Fagerson et al[14]
Acetic Acid	-432.2	0.2835	Fagerson et al[14]
Furan	-34.8	0.2672	Fagerson et al[14]

Table _: Most prominent organic products of fructose pyrolysis, along with relevant thermodynamic properties. Properties were found in the "Standard Thermodynamic Properties of Chemical Substances" table from the University of Indiana department of chemistry[6].

In order to quantify the graphitic carbon formed during the decomposition of fructose, it is necessary to determine the Gibb's free energy of each decomposition product forming. A hypothetical reaction was devised for each product to determine the stoichiometry and additional products (e.g. H_2O, CO_2, and CO) that would be necessary for a full thermodynamic analysis. These reaction products are summarized in Table_. It is worth noting at this point that for fructose, out of twelve decomposition reactions, only five have the stoichiometric ability to produce graphitic carbon.

Balanced Reactions (Oxygen Compounds)	**Balanced Reactions (Non-Oxygen Compounds)**
Acetaldehyde Reaction	Benzene Reaction
$2\ C_6H_{12}O_6 \rightarrow 6\ C_2H_4O\ \ 3\ O_2$	$2\ C_6H_{12}O_6 \rightarrow 2\ C_6H_6\ \ 6\ H_2O$
Acetone Reaction	Toluene Reaction
$C_6H_{12}O_6 \rightarrow 2\ C_3H_6O\ \ 2\ O_2$	$2\ C_6H_{12}O_6 \rightarrow C_7H_8\ \ 6\ H_2O\ \ 5\ C_{(s)}\ \ 2\ H_2$
Ethanol Reaction	Ethylbenzene Reaction
$C_6H_{12}O_6 \rightarrow 2\ C_2H_6O\ \ 2\ CO_2$	$2\ C_6H_{12}O_6 \rightarrow C_8H_8\ \ 6H_2O\ \ 4\ C_{(s)}\ \ H_2$
Acetic Acid	Styrene Reaction
$C_6H_{12}O_6 \rightarrow 2\ C_2H_4O_2\ \ 2\ CO\ \ H_2\ \ H_2O$	$2\ C_6H_{12}O_6 \rightarrow C_8H_8\ \ 6\ H_2O\ \ 4\ C_{(s)}\ \ 2\ H_2$
Furan Reaction	Indene Reaction
$C_6H_{12}O_6 \rightarrow C_4H_4O\ \ 3\ H_2O\ \ 2\ CO_2\ \ H_2$	$2\ C_6H_{12}O_6 \rightarrow C_9H_8\ \ 6\ H_2O\ \ 3\ C_{(s)}\ \ 2\ H_2$
Phenol Reaction	Graphite Reaction
$C_6H_{12}O_6 \rightarrow C_6H_6O\ \ 3\ H_2O\ \ O_2$	$C_6H_{12}O_6 \rightarrow 6\ C_{(s)}\ \ 6\ H_2O$

Table_: Balanced chemical reactions for the twelve main products of fructose decomposition. Note that only toluene, ethylbenzene, styrene, indene, and graphite reactions produce graphitic carbon.

After the stoichiometry of these reactions weas determined, the Gibb's free energy of each reaction (ΔG_r) was calculated and plotted against temperature, using the following equations:

$$\Delta G_f = \Delta H_f - T\Delta S_f$$

$$\Delta G_r = \sum \Delta G_{f,products} - \sum \Delta G_{f,reactants}$$

Where ΔHf is the standard enthalpy of formation, ΔSf is the standard molar entropy of the compound and T is temperature. ΔHf and ΔSf for most of the compounds were found in the literature and are summarized in Table_. ΔSf for fructose could not be found in the literature, so it was assumed to be the same as that of glucose (since the difference between the two compounds is minimal). The calculated Gibb's free energies were then used to determine if the formation of each product was thermodynamically favorable (and at what temperature).

1-pyrenebutyric acid was analyzed in a similar manner to fructose in order to compare their viabilities as carbon precursor options. Two assumptions were made for the PyBA model. First, it was assumed that the primary volatile organic products would be the same for PyBA as for fructose. Again, it is to be noted

that analyzing every conceivable product is unnecessary. The second assumption is based on the fact that no literature values could be found for the ΔHf and ΔSf of PyBA. This was calculated by assuming that the ΔGr was similar for the synthesis of PyBA from pyrene and butyric acid and the synthesis of 1-phenylbutyric acid from benene and butyric acid. The reactions are shown in Scheme 1.

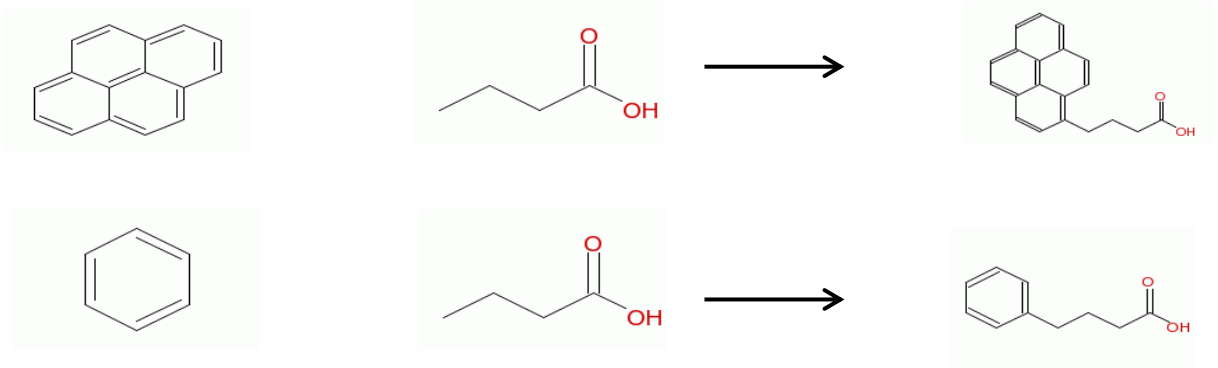

Scheme 1_: Two reactions that were assumed similar in order to determine thermodynamic properties of 1-pyrenebutyric acid.

The product summary for PyBA is shown in Table_. Again, it is important to note that, due to the fact that PyBA contains 20 carbon atoms in the structure, none of the decomposition reactions can be balanced without forming graphitic carbon.

Balanced Reactions (Oxygen Compounds)					**Balanced Reactions (Non-Oxygen Compounds)**					
Acetaldehyde Reaction					Benzene					
$C_{20}H_{16}O_2$	→	2 C_2H_4O	2 CH_4	14 C	$C_{20}H_{16}O_2$	→	2 C_6H_6	CH_4	CO_2	6 C
Acetone Reaction					Toluene					
$C_{20}H16O2$	→	2 C_3H_6O	CH_4	13 C	$C_{20}H_{16}O_2$	→	2 C_7H_8	CO_2	5 C	
Ethanol Reaction					Ethylbenzene					
$C_{20}H_{16}O_2$	→	2 C_2H_6O	CH_4	15 C	$C_{20}H_{16}O_2$	→	C_8H_{10}	$2H_2O$	H_2	12 C
Acetic Acid					Styrene					
$C_{20}H_{16}O_2$	→	$C_2H_4O_2$	3 CH_4	15 C	$C_{20}H_{16}O_2$	→	2 C_8H_8	CO_2	4 C	
Furan Reaction					Indene					
$C_{20}H_{16}O_2$	→	2 $C_4H_4O_2$	2 CH_4	10 C	$C_{20}H_{16}O_2$	→	2 C_9H_8	CO_2	C	
Phenol Reaction					Graphite					
$C_{20}H_{16}O_2$	→	2 C_6H_6O	CH_4	7 C	$C_{20}H_{16}O_2$	→	17 C	2 H_2O	3 CH_4	

Table 3: Balanced chemical reactions for the twelve main products of 1-Pyrenebutyric acid decomposition. Note that, contrary to fructose decomposition, all twelve products produce graphitic carbon.

The Gibb's free energies of these reactions were then plotted against temperature for both potential carbon precursors.

Carbon Precursor Absorption

As described by the thermodynamic study, 1-pyrenebutyric acid (PyBA) was determined to be the carbon source that most adequately meets the necessary criteria that is required to synthesize carbon nanotubes via this process. Three different methods of absorption were attempted to get the PyBA into the pores of the zeolite and the best method was determined by percent graphitic carbon residue obtained from thermogravimetric analysis (TGA).

Solution-based Absorption

Prior to being absorbed with carbon precursor, VPI-5 crystals were dried in a vacuum oven overnight. 50mg of VPI-5 was then immersed in a 10mM solution of 1-pyrenebutyric acid in acetone. The sample was then stirred in this solution for three hours. Crystals were then collected via vacuum filtration and dried in the vacuum oven overnight.

Sublimation Infiltration (Mechanically Mixed)

50mg of VPI-5 crystals were first mechanically mixed with 10mg of PyBA by grinding together with a mortar and pestle. The mixture was then transferred to an alumina boat and placed inside a tube furnace. Vacuum was pulled inside the furnace and the temperature was raised from room temperature to 100°C at a rate of ~2°C/min. Sample was held at 100°C for 1 hour to purge out any water that may be trapped within the pores of the zeolite. Since PyBA sublimes at 150°C at low pressures[citation needed], furnace was then ramped to 150°C at ~2°C/min and held at this temperature while maintaining vacuum for 4 hours. The mixture was then cooled to room temperature, washed with acetone, and dried overnight.

Sublimation Infiltration (With Porous AAO Barrier)

10mg PyBA was placed at the bottom of an alumina boat. A piece of porous alumina (AAO) membrane was placed on top of the PyBA powder, and 50mg VPI-5 crystals was placed on top of the AAO membrane. Boat was then placed inside the tube furnace and vacuum was pulled on the sample. Temperature of the furnace was then raised to from room temperature to 100°C at a rate of 2°C/min and held at this temperature for 1 hour to remove any water from the zeolite. Temperature was then raised to 150°C at a rate of 2°C/min and held at this temperature under vacuum for 4 hours before being cooled back down to room temperature. VPI-5 was then removed from top of the AAO barrier.

Pyrolysis

A general overview of the pyrolysis procedure goes as such. A sample of VPI-5 loaded with catalyst nanoparticles and carbon precursor was put in an alumina boat that was subsequently placed in a tube furnace. The furnace was then attached to a double bubbler and purged with argon five times by alternately pulling vacuum and flowing argon gas in the furnace. The temperature was then raised to 100°C and held at this temperature for 1 hour to purge out any water that may be trapped within the pores of the zeolite. After the water purge step, the temperature of the furnace was raised to the pyrolysis temperature at a rate of 10°C/min and held at that temperature for 1 hour before being cooled back down to room temperature. The appropriate temperature for pyrolysis was determined by treating

the zeolite that was not loaded with cobalt or carbon precursor to various temperatures between 600 and 1000°C. XRD was then taken of the zeolite after this annealing to determine if the VPI-5 retained the pore structure necessary for carbon nanotube synthesis.

Post Pyrolysis Treatment

After pyrolysis, the zeolite structure was dissolved away by immersing in the sample in 10% hydrochloric acid (HCl) and stirring for 1 hour.

As will be discussed in the results and discussion section, Raman spectroscopy indicated that carbon nanotubes ~0.8nm in diameter were present in multiple samples. Due to large amounts of amorphous carbon that was also present in the samples, transmission electron microscopy (TEM) was not able to confirm the presence of these CNTs via direct imaging. Several different post-pyrolysis treatments were applied to the samples in order to improve the chances of seeing CNTs using TEM.

Based on the principle that hydrogen peroxide (H_2O_2) oxidizes amorphous carbon at a higher rate than carbon nanotubes and will not damage the zeolite structure[10], it was proposed that the concentration of CNTs relative to amorphous carbon could be improved by treating the pyrolyzed carbon product with H_2O_2 prior to dissolving the zeolite in HCl to remove any carbon product that was formed on the outside of the zeolite and leave the CNTs that were formed within the pores intact.

Another tactic for making CNTs more visible using TEM was to add Triton surfactant to the liquid mixture during ultrasonication.

Characterization

X-Ray Diffraction (XRD)

A Siemens D500 Powder X-ray diffractometer (XRD), operating with Cu Kα radiation (λ=1.5408Å) was used to characterize the synthesized VPI-5. A 2θ scan from 4° to 40° at a rate of 1.0° per minute was used.

Scanning Electron Microscopy (SEM)

Scanning electron microscopy was used to image the VPI-5 crystals and was carried out on an S-4300 Hitachi microscope. All zeolite samples were sputter coated with gold prior to analysis.

Micro-Raman Spectroscopy

Raman spectroscopy was used to characterize carbon nanotubes. Analysis was carried out using a dispersive Micro-Raman spectrometer from Thermo Scientific using 780nm laser excitation.

Thermogravimetric Analysis (TGA)

TGA was used to determine graphitic carbon content of the zeolite after various absorption processes. TGA was run on a NETZSCH STA449C thermal instrument. The sample was heated from room temperature to 1000°C at a rate of 10°C/min under flowing nitrogen (20 cm^3/min), followed by a carbon

burn at 1000°C with flowing air for 30 minutes. The graphitic carbon content was determined by the weight loss associated with this final carbon burn.

- Since VPI-5 is not commercially available, it must first be synthesized using the procedure described by Anderson, et al[6]
- Vacuum dry to remove all water from zeolite, as it decomposes at high temperature in the presence of water[5,6]
- Infiltrate VPI-5 with 1-pyrenebutyric acid via low pressure, sublimation infiltration.
- Infiltrate VPI-5 with $CoCl_2$ via solution infiltration and reduce Co^{2+} to Co nanoparticles using $NaBH_4$[7]
- Pyrolyze carbon precursor within zeolite pores at high temperature under argon atmosphere
- Dissolve zeolite template away using HCl

Results and Discussion

Synthesis of VPI-5

Following the optimized procedure by Anderson, et al [5], VPI-5 was synthesized and characterized by x-ray diffraction (XRD) and scanning electron microscopy (SEM). Major diffraction peak for [100], representing the largest d-spacing in the structure, verifies that the pore structure we need for our synthesis is present, as shown in Figure 1. Subsequent XRD after various annealing temperatures confirm that zeolite retains its pore structure at pyrolysis temperature, provided the sample was thoroughly dried prior to being raised to this temperature.

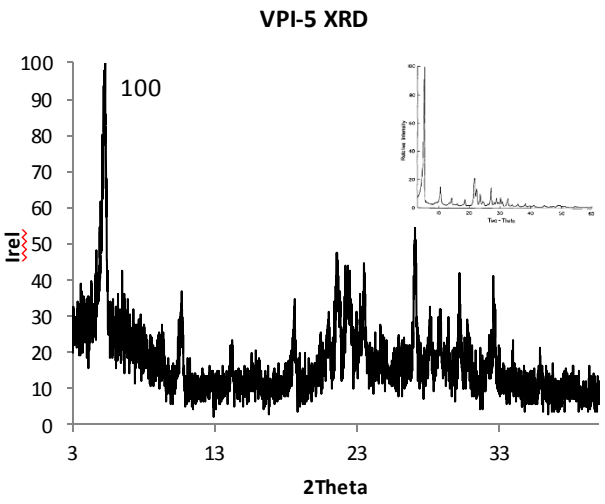

Figure 1: XRD plot of synthesized VPI-5, highlighting [100] peak. Crystalline data for VPI-5: a = b = 18.975 Å, c = 8.104 Å α = β = 90°, γ = 120°. Inset: reference VPI-5 XRD pattern[5]

Figure 2, the long, needle-like crystal structure that is characteristic of VPI-5 is clearly present.

SEM was also used to characterize VPI-5 by directly imaging the crystal to determine structure and estimate their length. As seen in

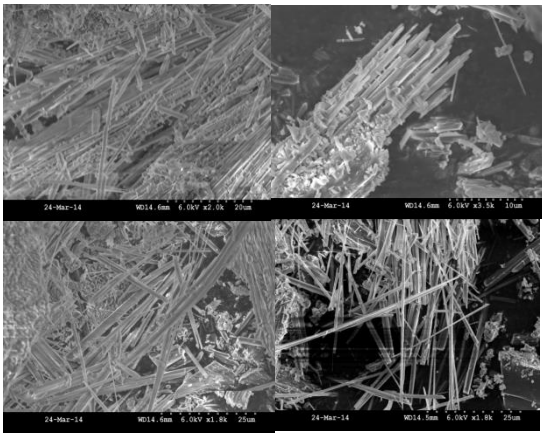

Figure 2: SEM images of VPI-5 crystals, confirming long, needle-like structure.

Thermodynamic Study of Carbon Precursors

Fructose

After all potential decomposition reactions were balanced, the Gibbs' free energy of formation was calculated for all products, including numerous small molecules, such as carbon dioxide, water, and methane, using the equations listed previously along with literature values for enthalpy of formations and standard molar entropy. Since the CNT synthesis reaction involves temperatures up to about 1250 K, the temperature was varied from room temperature to 1250 K. the free energies of the oxygen-containing and non-oxygen –containing products are shown in Tables_ and _ respectively.

	Acetaldehyde	Acetone	Ethanol	Acetic Acid	Furan	Fructose	Carbon Dioxide	Water	Oxygen	Phenol	Carbon Monoxide
T (K)	ΔGf	ΔGf	ΔGf	ΔGf	ΔGf	ΔGf	ΔGf	ΔGf	ΔGf	ΔGf	ΔGf
300	-245.34	-305.69	-319.28	-512.36	-114.96	-1333.7600	-457.4	-298.2	-61.5	-208.2	-169.6
350	-258.53	-320.455	-333.36	-525.72	-128.32	-1344.2200	-468.05	-307.6	-71.75	-215.4	-179.45
400	-271.72	-335.22	-347.44	-539.08	-141.68	-1354.6800	-478.7	-317	-82	-222.6	-189.3
450	-284.91	-349.985	-361.52	-552.44	-155.04	-1365.1400	-489.35	-326.4	-92.25	-229.8	-199.15
500	-298.1	-364.75	-375.6	-565.8	-168.4	-1375.6000	-500	-335.8	-102.5	-237	-209
550	-311.29	-379.515	-389.68	-579.16	-181.76	-1386.0600	-510.65	-345.2	-112.75	-244.2	-218.85
600	-324.48	-394.28	-403.76	-592.52	-195.12	-1396.5200	-521.3	-354.6	-123	-251.4	-228.7
650	-337.67	-409.045	-417.84	-605.88	-208.48	-1406.9800	-531.95	-364	-133.25	-258.6	-238.55
700	-350.86	-423.81	-431.92	-619.24	-221.84	-1417.4400	-542.6	-373.4	-143.5	-265.8	-248.4
750	-364.05	-438.575	-446	-632.6	-235.2	-1427.9000	-553.25	-382.8	-153.75	-273	-258.25
800	-377.24	-453.34	-460.08	-645.96	-248.56	-1438.3600	-563.9	-392.2	-164	-280.2	-268.1
850	-390.43	-468.105	-474.16	-659.32	-261.92	-1448.8200	-574.55	-401.6	-174.25	-287.4	-277.95
900	-403.62	-482.87	-488.24	-672.68	-275.28	-1459.2800	-585.2	-411	-184.5	-294.6	-287.8
950	-416.81	-497.635	-502.32	-686.04	-288.64	-1469.7400	-595.85	-420.4	-194.75	-301.8	-297.65
1000	-430	-512.4	-516.4	-699.4	-302	-1480.2000	-606.5	-429.8	-205	-309	-307.5
1050	-443.19	-527.165	-530.48	-712.76	-315.36	-1490.6600	-617.15	-439.2	-215.25	-316.2	-317.35
1100	-456.38	-541.93	-544.56	-726.12	-328.72	-1501.1200	-627.8	-448.6	-225.5	-323.4	-327.2
1150	-469.57	-556.695	-558.64	-739.48	-342.08	-1511.5800	-638.45	-458	-235.75	-330.6	-337.05
1200	-482.76	-571.46	-572.72	-752.84	-355.44	-1522.0400	-649.1	-467.4	-246	-337.8	-346.9
1250	-495.95	-586.225	-586.8	-766.2	-368.8	-1532.5000	-659.75	-476.8	-256.25	-345	-356.75

Table_: Calculated Gibbs' free energies of formation for all oxygen containing products of fructose decomposistion.

	Benzene	Toluene	Ethylbenzene	Styrene	Indene	Graphite	Hydrogen	Methane
T (K)	ΔGf	ΔGf	ΔGf	ΔGf	ΔGf	ΔGf	ΔGf	ΔGf
300	-4.19	-54.3	-64	32	46.01	-1.71	-39	-130.49
350	-13.055	-65.35	-76.75	20.1	35.245	-1.995	-45.5	-139.805
400	-21.92	-76.4	-89.5	8.2	24.48	-2.28	-52	-149.12
450	-30.785	-87.45	-102.25	-3.7	13.715	-2.565	-58.5	-158.435
500	-39.65	-98.5	-115	-15.6	2.95	-2.85	-65	-167.75
550	-48.515	-109.55	-127.75	-27.5	-7.815	-3.135	-71.5	-177.065

600	-57.38	-120.6	-140.5	-39.4	-18.58	-3.42	-78	-186.38
650	-66.245	-131.65	-153.25	-51.3	-29.345	-3.705	-84.5	-195.695
700	-75.11	-142.7	-166	-63.2	-40.11	-3.99	-91	-205.01
750	-83.975	-153.75	-178.75	-75.1	-50.875	-4.275	-97.5	-214.325
800	-92.84	-164.8	-191.5	-87	-61.64	-4.56	-104	-223.64
850	-101.705	-175.85	-204.25	-98.9	-72.405	-4.845	-110.5	-232.955
900	-110.57	-186.9	-217	-110.8	-83.17	-5.13	-117	-242.27
950	-119.435	-197.95	-229.75	-122.7	-93.935	-5.415	-123.5	-251.585
1000	-128.3	-209	-242.5	-134.6	-104.7	-5.7	-130	-260.9
1050	-137.165	-220.05	-255.25	-146.5	-115.465	-5.985	-136.5	-270.215
1100	-146.03	-231.1	-268	-158.4	-126.23	-6.27	-143	-279.53
1150	-154.895	-242.15	-280.75	-170.3	-136.995	-6.555	-149.5	-288.845
1200	-163.76	-253.2	-293.5	-182.2	-147.76	-6.84	-156	-298.16
1250	-172.625	-264.25	-306.25	-194.1	-158.525	-7.125	-162.5	-307.475

Table 4: Calculated Gibbs' free energies of formation for all non-oxygen-containing products of fructose decomposition.

These Free energies were then used to calculated the Gibbs' free energy of each decomposition reaction at the various temperatures using the above ΔGr equation (with ΔGf of products and reactant adjusted for stoichiometry). The calculated ΔGr were then plotted for fructose as shown in Figure 3.

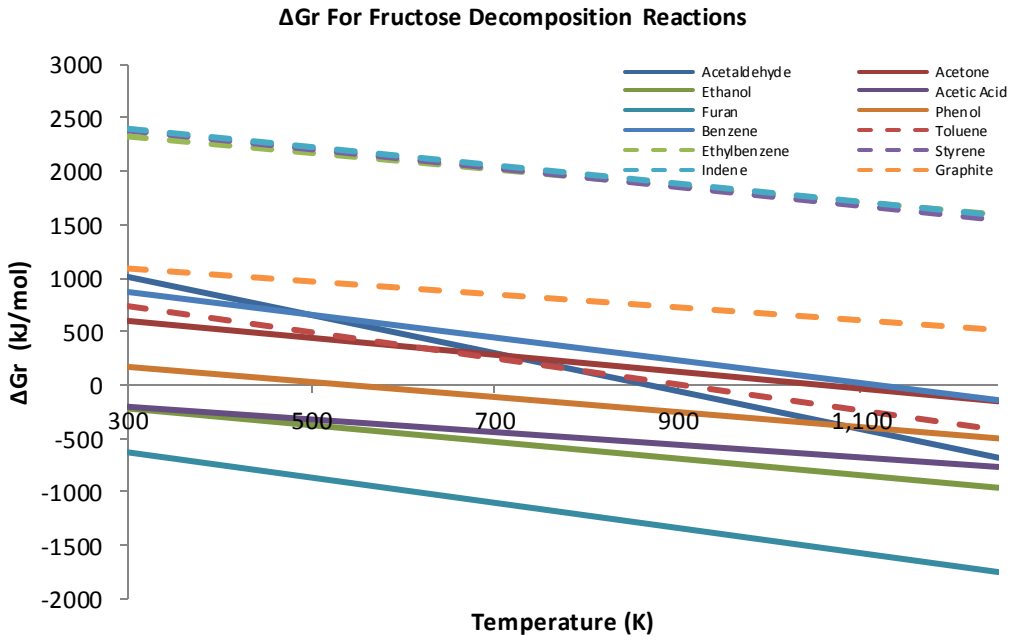

Figure 3: Gibbs' free energy of reaction for the twelve fructose decomposition reactions. Note that negative ΔGr does not necessarily require that reaction proceeds at room temperature. Analysis does not take kinetic limitations into account. Dashed lines are the reactions of interest that produce graphitic carbon and aromatics that can polymerize. Graphite reaction is ideal for producing CNTs.

The five reactions that produce graphitic carbon are shown by the dashed lines in the figure 3. Of those five reactions, only one is thermodynamically favorable at the temperatures being used for CNT synthesis, which explains the low carbon yield that was produced when fructose is pyrolyzed. Based on this analysis, there are two primary factors that negatively affect the carbon yield of this process. The first is the highly negative ΔGf of fructose (<-1300kJ/mol) at room temperature prevents most of the carbon producing reactions from being favorable within the required temperature range. The second is the numerous oxygen atoms present in the fructose molecule. This high oxygen/carbon ratio means that more of the carbon will be released in the form of volatile organics and carbon dioxide, rather than being left behind as graphitic carbon residue. This fits well with experimental observation of negligible residual mass after annealing. Using this information, we were able to add two new criteria to the precursor selection process. The ideal precursor must have a ΔGf that is significantly less negative than fructose, allowing it to more readily decompose within the necessary temperature range. It also most have a high carbon/oxygen ratio in order to minimize the amount of carbon lost to organics and CO_2.

1-Pyrenebutyric Acid

Based on our newly added criteria, 1-pyrenebutyric acid (PyBA) appears to be a much more viable candidate as a carbon precursor than fructose. The alkyloic acid group attached the the pyrene means that it will still be hydrophilic and thus, can still be absorbed into the pores of the zeolite. Add to that the fact that PyBA has an approximate ΔGf that is significantly less negative (~-275 kJ/mol) at room temperature than fructose and has a much higher ratio of carbon atoms to oxygen atoms in the structure (20:2).

Again, the ΔGr for the formation of each compound was plotted against temperature from 300-1250 K. The results of which are shown in Figure 4.

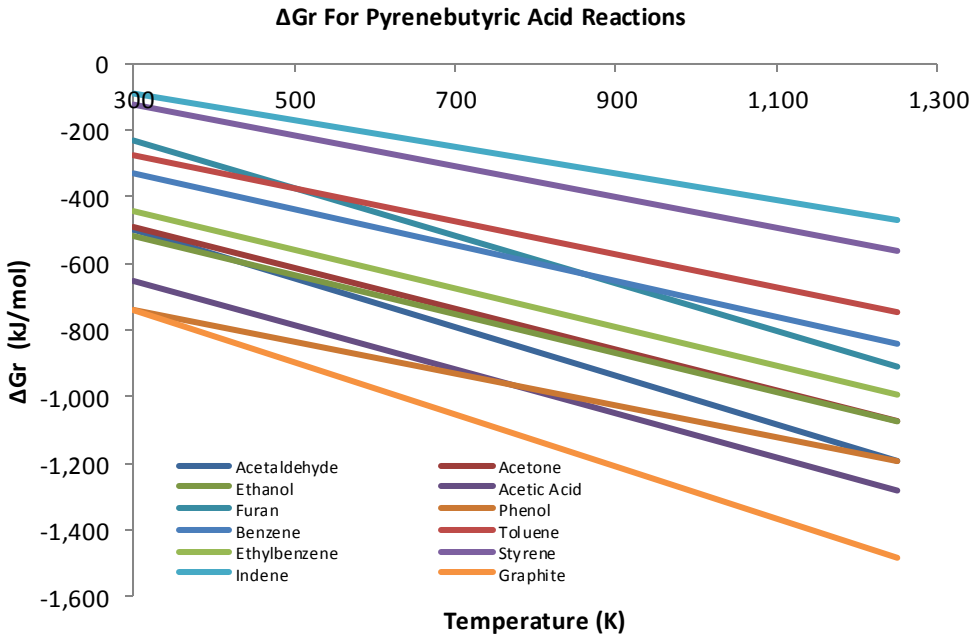

Figure 4: Gibbs' free energy of reaction for the twelve PyBA decomposition reactions. Note that negative ΔGr does not necessarily require that reaction proceeds at room temperature. Analysis does not take kinetic limitations into account. Due to high carbon content of PyBA, all reactions form graphitic carbon in some quantity and all reactions are thermodynamically favorable due to the low –ΔHf of PyBA.

It is immediately noticeable that all reactions are thermodynamically (albeit not necessarily kinetically) favorable over the entirety of the required temperature range. Add to that the fact that all of the reactions involved produce graphitic carbon and one would expect a significantly higher amount of graphitic carbon residue in the product and thus, would work better as a carbon precursor than fructose.

Thermogravimetric Analysis (TGA)

Thermogravimetric analysis (TGA) was used to determine the best method of absorption for the carbon precursors by determining how much graphitic carbon could be produced from each absorption method. Each method showed three consistent stages, regardless of the absorption method, catalyst, and carbon precursor employed.

The first stage was the small weight loss around 100°C. This loss was due to the evaporation of residual water that was absorbed into the VPI-5 pores. This result showed that it was necessary to add the water-purge stage to the beginning of the pyrolysis procedure.

The second distinct stage of the TGA experiment was the stage that involved the largest mass drop of the overall procedure and occurred between 250-600°C. This distinct region of the plot was due to the formation (and subsequent evaporation) of the various volatile organic compounds formed from the pyrolysis of the carbon precursor (As detailed in the thermodynamic analysis section).

The final stage of the experiment involved minimal weight loss after all of the volatile organics evaporated, from 600-1000°C, followed by a sudden weight loss at 1000°C after the introduction of air into the system. This section of the plot is the most important, as it determines (A) The lower limit of pyrolysis temperature, (B) The total percentage of carbon precursor that was absorbed into the sample, and (C) The weight percent of graphitic carbon that could be extracted from the conditions tested.

Carbon Precursor Absorption

PyBA was infiltrated into the VPI-5 using vacuum sublimation infiltration, using an AAO membrane as a barrier between unevaporated PyBA and VPI-5. Thermogravimetric analysis (TGA) was used to quantify graphitic carbon that could be created using this precursor and method of infiltration. The specimen was raised to pyrolysis temperatures under an inert N2 atmosphere at 10C/min. When pyrolysis temperature was reached, air was allowed into the system to burn away remaining carbon. The drop in mass percent was used to quantify the percentage of amorphous carbon that was absorbed in the zeolite. The mass drop was found to be about 3% before the cobalt was added and about 1% after the cobalt was added. Though, the cobalt drop is misleading, as it was affected by the mass increase due to the oxidation of the cobalt nanoparticles.

Determination of Optimal Pyrolysis Temperature

Since VPI-5 is not stable at high temperatures[citation needed], it was necessary to determine the highest temperature at which the pyrolysis process could be carried out. To do this, the zeolite was annealed in an inert, argon atmosphere to various temperatures between 600-1000°C, with a hold at 100°C to purge any water prior to ramping to annealing temperature. X-ray diffraction patterns were then taken for each sample to determine if they retained the characteristic (100) diffraction peak, showing that they still had the 1.2nm pore that is required for synthesis of 0.8nm carbon nanotubes.

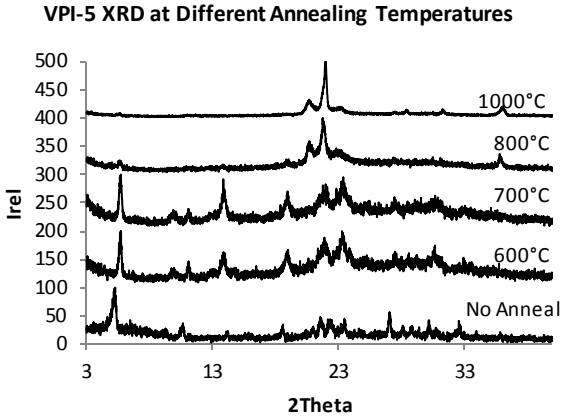

The XRD data collected shows that the (100) diffraction peak is completely removed when the temperature of the zeolite is raised above 700°C, even when all water is purged from the pores and no carbon precursor is absorbed into the sample.

TGA Determination of Optimum Absorption Procedure

Raman Spectroscopy of Pyrolysis Product

Raman spectroscopy is the most widely used characterization method for identification of carbon nanotubes[8,11]. Several characteristic bands can be used to identify the presence of single-walled carbon nanotubes, such as the vibration of the hexagonal structure of graphitic carbon (G-band) and the vibration that is induced by defects in the graphitic structure (D-band). The most informative band however, is the radial breathing mode (RBM) of the Raman spectrum. As the name suggests, this band is due to the wall of the CNT vibrating radially outward and inward ("breathing"). This band can be used, not only to distinguish the Raman spectrum of CNTs from graphitic carbon, but also to measure their approximate diameter. The ideal CNT sample will contain a large ratio between the heights of the G-band to the D-band and will also show a well-defined, narrow RBM peak at ω=397cm^{-1}.

The various synthesis parameters were evaluated on their ability to produce carbon nanotubes based on the Raman spectra obtained from the final product. The results are summarized in Table_.

Sample	Catalyst	Reduced	Catalyst In/Out	Abs with AAO	H_2O_2 Oxidation	Surfactant	G/D	RBM
1	Co	x	In	x			0.98	None
2	Co	x	Out	x			0.97	None
3	Co	x	In	x	x		0.97	Weak
4	Co	x	Out	x	x		1.05	None

5	Co	x	In	x	x	x	None	None
6	Co	x	Out	x	x	x	1	None
7	Co	x	In		x		1.16	None
8	Co	x	In				1.19	None
9	Fe	x	In	x	x			None
10	Fe	x	In	x			None	None
11	Fe		In	x	x			None
12	Fe		In	x				None
Best	Co	x	In				1.42	Strong/Broad

Table _: Summary of Raman results for various experimental parameters, such as element and oxidation state of the transition metal catalyst, method of carbon precursor absorption, and post-pyrolysis treatments.

Best CNT Synthesis Procedure

Based on the Raman spectroscopic results obtained from altering the various synthesis parameters, the samples that most likely contain carbon nanotubes were synthesized using the following procedure.

VPI-5 zeolite was synthesized by the optimized procedure as described by Anderson, et al[5]. Zeolite crystals were then dried in a vacuum oven to remove any water from the pores. Sample was then immersed in solution of $CoCl_2$ and allowed to soak for 3 hours to absorb Co^{2+} ions into the pore structure of VPI-5. After the Co@VPI-5 crystals were filtered by vacuum filtration and dried in a vacuum oven, they were immersed in a solution of sodium borohydride ($NaBH_4$) in water to reduce Co^{2+} ions to Co nanoparticles. These crystals were then collected by vacuum filtration and dried in a vacuum oven overnight. Sample was then mechanically mixed with 1-pyrenebutyric acid (PyBA) and placed in an alumina boat before being transferred into the tube furnace. The tube furnace was then placed under vacuum using a vacuum pump. The sample was then heated to 100°C at a rate of 2°C/min and maintained at that temperature and pressure for 1 hour, before raising the temperature to 150°C at a rate of 2°C/min and holding for 4 hours. After they were cooled to room temperature, the VPI-5 crystals were removed from the furnace and excess PyBA was washed from the surface with acetone. Co@VPI-5 with PyBA inside pores was then placed back in the alumina boat in the furnace and was purged 5 times using argon gas. The temperature was raised to 650°C under flowing argon (again, with a 100°C water purge step) and held at this temperature for 1 hour. After it was cooled back to room temperature, the product was recovered and placed in 10% HCl to dissolve away the zeolite template.

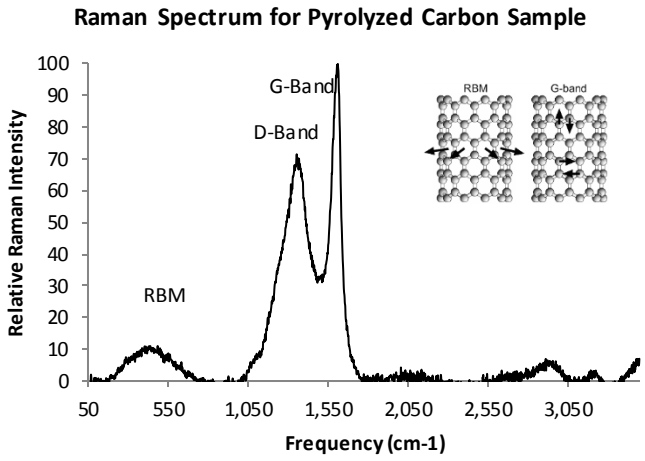

Figure 6: Raman spectrum of pyrolyzed carbon sample, showing graphite-related (G-band), defect-induced (D-band), and Radial Breathing Mode (RBM). Inset: diagram of RBM and G-band.

Raman spectrum of this sample showed the largest G/D ratio among all synthesis

attempts along with the most well-defined RBM peak, showing strong promise to the presence of 0.8nm single-walled carbon nanotubes.

Conclusions

References

[1] Hinds et al, *Nature* **2005,** 438*,* 44

[2] Corry, B *J. Physical Chemistry*, **2008,** *112,* 1427-1434

[3] Magrez et al, *Materials,* **2010**, 3, 4871-4891

[4] Zhai, J.P et al, *Nature*, **2000**, 408, 50-51

[5] Davis, M et al, *Zeolites*, **1988**, 8, 362-366

[6] Anderson et al, *Zeolites* **1996,** *16,* 15-21

[7] Rakap et al, *Applied Catalysis B: Environmental*, **2009**, 91, 21-29

[8] Maultzsch et al, *Physical Review B*, **2005**, 72, 205438

[9] Prasad, S, *Microporous Materials*, **1997**, 12, 123-130

[10] Feng, et al, *ACS Nano*, **2008**, 2, 1634-1638

[11] Dresselhaus et al, *Carbon*, **2002**, 40, 2043-2061

[12] University of Indiana Dept of Chemistry. "Standard Thermodynamic Properties of Chemical Substances." http://courses.chem.indiana.edu/c360/documents/thermodynamicdata.pdf

[13] Higman, E.B., et al. *Journal of Agricultrual and Food Chemistry*, **1970**, 18, 636-640.

[14] Fagerson, I.S., et al. *Journal of Agricultural and Food Chemistry*, **1969**, 16, 747-750.